Materials Today Communications 33 (2022) 104436

Contents lists available at ScienceDirect

Materials Today Communications

journal homepage: www.elsevier.com/locate/mtcomm

Relation between cation distribution and chemical bonds in spinel $NiFe_2O_4$

Ying Fang, Siming Zhang, Paul R. Ohodnicki, Guofeng Wang *

Department of Mechanical Engineering and Materials Science, University of Pittsburgh, Pittsburgh, PA 15261, USA

ARTICLE INFO

Keywords:
Density functional theory
Machine learning
Spinel crystal
$NiFe_2O_4$
Cation distribution

ABSTRACT

In spinel oxides, the cation distribution plays an important role in determining their technologically important properties. Herein computational predictions based on the first principles calculations are presented to elucidate the relation between cation distribution and chemical bonds in spinel $NiFe_2O_4$. The variation of physical properties (such as system energy, lattice parameter, and atomic magnetic moment) with respect to the cation distribution (i.e., degree of inversion) in spinel $NiFe_2O_4$ oxide is discussed. This study further reveals that the energy of spinel $NiFe_2O_4$ oxide is linearly proportional to the number of different types of cation-oxygen-cation bonds in the spinel structure. The equilibrium degree of inversion in spinel $NiFe_2O_4$ at elevated temperatures and the transformation from an ordered to disordered cation distribution in inverse spinel $NiFe_2O_4$ are predicted and found to be driven by competition between bond enthalpy and entropy of cation site occupancy.

1. Introduction

Spinel ferrites with a general chemical formula of AFe_2O_4 (A = Mn, Co, Ni, Cu, or Zn) have interesting and technologically relevant magnetic and electrical properties [1,2]. In particular, nickel ferrite ($NiFe_2O_4$) displays properties of high saturation magnetization [3], high surface reactivity [4], high sensing sensitivity toward gases such as hydrogen sulfide and acetone [5], outstanding capacity [6], and impressive electrochemical stability [7]. Hence, $NiFe_2O_4$ becomes an attractive candidate for a wide range of applications such as photocatalysts [8,9], catalysts [4], gas sensors [10] and electrodes [11,12].

The crystal structure of spinel $NiFe_2O_4$ can be viewed as a superlattice consisting of eight (2x2x2) face-centered cubic unit cells with the lattice sites occupied by oxygen ions. In addition, one eighth of the tetrahedral and one half of the octahedral sites of the lattice are occupied by the Ni and Fe cations. In a normal spinel structure, all Ni ions will lie at the tetrahedral sites whereas all Fe ions at the octahedral sites. By contrast, half of the Fe ions will lie at the tetrahedral sites, whereas the octahedral sites are occupied by both Ni and Fe ions in an inverse spinel structure. Varying from the normal to inverse structures, spinel $NiFe_2O_4$ can be expressed in general formula of $\left(Ni^{2+}_{1-x}Fe^{3+}_{x}\right)_T\left(Ni^{2+}_{x}Fe^{3+}_{2-x}\right)_O O_4$, where T and O represent tetrahedral and octahedral cation sites, respectively. Degree of inversion (denoted as x) of a spinel $NiFe_2O_4$ can thus be quantified as the fraction of the tetrahedral sites occupied by Fe ions and has a value ranging from $x = 0.0$ for a normal structure to $x = 1.0$ for an inverse structure.

It has been found that cation distribution in the spinel lattice could affect the structure, morphology, and physical/chemical properties of $NiFe_2O_4$ crystal [13–15]. Cvejić et al. prepared $NiFe_2O_4$ nanopowder samples using a co-precipitation and subsequent annealing procedure [16]. They observed that the samples annealed at different temperature had different degree of cation distribution and the magnetization of $NiFe_2O_4$ could vary from 12 emu·g^{-1} for a fully inverse spinel structure to 38 emu·g^{-1} for a partially inverse spinel structure. Moreover, El-Sayed et al. synthesized the $NiFe_2O_4$ samples using a sol gel method and found that an increase in annealing temperature would lead to enhanced migration of nickel ions from the tetrahedral sites to the octahedral sites of the spinel lattice [17]. This cation distribution change was correlated with an increase in the magnetization of the $NiFe_2O_4$ samples and this study thus provided for an opportunity to experimentally probe the dependence of magnetic property on cation distribution.

Many experimental characterization techniques have been applied to accurately measure the cation distribution in spinel crystal. For example, Šepelák et al. demonstrated that the cation distribution in $NiFe_2O_4$ could be quantified from Mössbauer spectra [14]. In addition, X-ray photoelectron spectroscopy (XPS) can be used to determine the degree of the cation distribution in spinel [18]. In comparison, the computational methods for quantitative prediction of cation distribution in spinel crystal as a function of temperature have not been well established yet. Various factors, such as crystal field splitting [19], local electrostatic effect [20], and pseudopotential orbital radii [21], have

* Corresponding author.
E-mail address: guw8@pitt.edu (G. Wang).

https://doi.org/10.1016/j.mtcomm.2022.104436
Received 31 May 2022; Received in revised form 5 September 2022; Accepted 9 September 2022
Available online 12 September 2022

been adopted to qualitatively explain the tendency of cation distribution in a spinel crystal. Tang et al. proposed a quantum mechanical approach for quantitively estimating the degree of cation distribution in spinel ferrite based on the cation ionization energy, cation-anion distance, Pauli repulsion energy, magnetic ordering energy, and tendency toward charge density balance [22]. However, this computational approach gave a seriously underestimated value of 0.7594, as compared to experimental value about 1.0 [17,23], for the cation distribution in $NiFe_2O_4$ after a correction term for ionicity was included [24]. Hence, a new theoretical framework is needed to correlate degree of cation distribution with the structural features of spinel crystal.

In this study, the first-principles density functional theory (DFT) calculations have been performed to predict how the material properties of spinel $NiFe_2O_4$ would vary with changes in cation distribution (i.e., degree of inversion). Moreover, analysis of the type and number of chemical bonds in spinel $NiFe_2O_4$ with different degrees of inversion was conducted. Furthermore, machine learning techniques were used to derive the relation between the system energies and chemical bonds of the crystal and this relation was used to predict the equilibrium cation distribution in spinel $NiFe_2O_4$. It should be mentioned that Pilania et al. have implemented a cluster expansion-enabled computational approach to predict the ordered ground state structure and cation ordering in double spinel compound $MgAlGaO_4$ [25]. Within the cluster expansion-based effective Hamiltonian approach, the energy of spinel crystal is expressed as a linear combination of the contributions from various cluster configurations. By contrast, a new computational approach, based on chemical bond analysis, is proposed here to elegantly elaborate on the relation between cation distribution and the underlaid chemical bonds and to reliably predict the cation distribution in spinel $NiFe_2O_4$ crystal.

2. Computational methods

2.1. DFT calculations

The first-principles spin-polarized calculations were performed using the Vienna Ab initio Simulation Package (*VASP*) [26]. Plane wave basis associated with the projector augmented wave approach was employed [27]. Exchange correlation was treated with generalized gradient approximation (GGA) in the form of Perdew-Birke-Ernzerhof (PBE) functional [28]. In all calculations, the plane-wave cut-off energy was set as 500 eV and the total energy of system was converged within 10^{-6} eV. As in GGA+U calculations, effective on-site Coulomb interaction parameter $U_{eff} = 4eV$ on Fe ions and $U_{eff} = 6.4eV$ on Ni ions were chosen. The structural optimization calculations used a $4 \times 4 \times 4$ Monkhorst-Pack k-point mesh [29]. All the structures were fully relaxed until the force acting on each atom was lower than 0.01 eV/Å. The special quasi-random structures (SQS) method implemented in Alloy Theoretic Automated Toolkit (*ATAT*) was used to construct the crystal structures that mimic the cation distribution in a random oxide [30].

2.2. Machine learning (ML)

Two different machine learning methods, linear regression and neural network as implemented in *scikit learn* [31], were employed to independently find the relation between the system energy and structural feature (i.e., chemical bonds) of spinel $NiFe_2O_4$ crystal with various cation distributions [32]. The linear regression by ordinary linear squares assumes linearity between structural features and target properties, whereas the neural network, in which fifty hidden layers with each hidden layer containing a hundred neurons were used, assumes a non-linear approximation for regression. Four-fold cross validation was applied in this work to evaluate the performance of machine learning methods. During the cross validation, the training dataset was randomly divided into four data folds. Three data folds were set as training dataset to train the machine learning model. The remaining data fold was the test dataset and used to examine the reliability of the machine learning model. The training error and test error were calculated as the root mean square error (RMSE) between the predicted and actual values of the training dataset and test dataset, respectively. This cross-validation procedure was repeated four times to ensure that each fold served as the test dataset once. The test error and training error of the cross-validation procedure was evaluated as the average value of the four test errors and training errors, respectively.

2.3. Monte Carlo simulation

The Monte Carlo (MC) simulation method based on the Metropolis algorithm was implemented to predict the cation distribution in spinel $NiFe_2O_4$ at thermodynamic equilibrium condition. Starting from a given initial structure containing eight formula of $NiFe_2O_4$, an attempt to swap the positions of a pair of randomly selected Ni and Fe ions is tried at each iteration. The energy associated with the structural change was calculated with the machine learning methods. A Boltzmann distribution-based probability (p) was used to determine the acceptance or rejection of the attempted structural change. Specifically, probability $p = \min\left[1, \exp\left(-\frac{\Delta E}{k_B T}\right)\right]$, where ΔE is the energy caused by the structural change, k_B is the Boltzmann constant and T is system temperature. The equilibrium degree of inversion of spinel $NiFe_2O_4$ was evaluated as the value averaged over 500 equilibrium structures sampled every 100 MC iterations during the last 50,000 iterations of the MC simulations at 1523 K and 1640 K. The ordering parameter of an inverse spinel $NiFe_2O_4$ was recorded every 100 MC iterations during the last 10,000 iterations of the MC simulations at the temperature range from 100 K to 230 K.

3. Results

3.1. DFT predicted properties of spinel $NiFe_2O_4$

The ground state magnetic ordering in the normal ($x = 0.0$) and inverse ($x = 1.0$) spinel $NiFe_2O_4$ has been determined in the previous computational studies [33–36]. However, the reports on the ground spin arrangement in spinel $NiFe_2O_4$ with a degree of inversion between these two cases (i.e., $0.0 < x < 1.0$) are currently missing in the literature. In this work, the system energies of all kinds of spinel $NiFe_2O_4$ with several possible spin arrangements were predicted and compared. The calculation results, as presented in Table 1, show clearly the ground state magnetic ordering to be one in which all the cations at the octahedral sites are of majority spin whereas all the cations at the tetrahedral sites are of minority spin in spinel $NiFe_2O_4$ with any degree of inversion (x). It should be mentioned that the predicted ground state magnetic orderings in $NiFe_2O_4$ are the same as the previous computational results for spinel $CoFe_2O_4$ [37].

In Table 2, the predicted lattice parameters of spinel $NiFe_2O_4$ with different degree of inversion are presented. These results show the lattice parameter decreases slightly from the normal to the inverse structures by about 0.94%, agreeing with previous computational results [38]. The calculation also predicts the lattice parameter of the inverse $NiFe_2O_4$ to be 8.41 Å, close to experimental values [16,17]. Moreover, the formation enthalpy of a spinel $NiFe_2O_4$ crystal with a given degree of inversion was calculated as the energy difference relative to that of the normal spinel $NiFe_2O_4$. The predicted formation enthalpy of spinel $NiFe_2O_4$ as a function of degree of inversion is plotted in Fig. 1. The DFT results exhibit a nearly linear relation between the calculated formation enthalpies and degree of inversion of spinel $NiFe_2O_4$. More importantly, the DFT energy calculation results show that a normal spinel $NiFe_2O_4$ ($x = 0.00$) would have system energy about 0.60 eV per formula unit (f. u.) higher than that of an inverse structure ($x = 1.00$), predicting that it is energetically favorable for the Ni ions to occupy the octahedral sites. The calculated energy difference is consistent with the previous

Table 1
Different possible spin arrangement, the resultant system energy and total magnetic moment in spinel $NiFe_2O_4$ with various degrees of inversion. Symbols ↑ and ↓ denote majority spin and minority spin, respectively. The system energies are given as the relative values with reference to the energy of $NiFe_2O_4$ with the ground magnetic ordering at a specified degree of inversion.

Degree of Inversion (x)	Ni at Tetrahedral Site	Ni at Octahedral Site	Fe at Tetrahedral Site	Fe at Octahedral Site	Energy (eV/f.u.)	Total Magnetic Moment (μ_B/f.u.)
0.00	↑	–	–	↑	1.518	12
0.00	↑	–	–	↑↓	0.005	2
0.00	↓	–	–	↑	0.000	8
0.25	↑	↑	↑	↑	0.473	12
0.25	↓	↓	↑	↑	0.235	8
0.25	↑	↑	↓	↑↓	0.076	2
0.25	↓	↑	↓	↑	0.000	6.5
0.50	↑	↑	↑	↑	0.407	12
0.50	↓	↓	↑	↑	0.286	8
0.50	↑	↑	↓	↑↓	0.098	2
0.50	↓	↑	↓	↑	0.000	5
0.75	↑	↑	↑	↑	0.643	12
0.75	↓	↓	↑	↑	0.358	8
0.75	↑	↑	↓	↑↓	0.139	2
0.75	↓	↑	↓	↑	0.000	3.5
1.00	–	↑	↑	↑	0.615	12
1.00	–	↓	↑	↑	0.407	8
1.00	–	↑	↓	↑	0.000	2

Table 2
Predicted lattice parameters of spinel $NiFe_2O_4$ with various degree of inversion.

Degree of inversion	Lattice parameter (Å)		
	GGA+*U* (this work)	GGA+*U* (Ref. [38])	Experiment
0.00	8.49	8.53	
0.25	8.47	–	
0.50	8.44	8.47	
0.75	8.42	8.45	
1.00	8.41	8.43	8.34 [16], 8.37 [17]

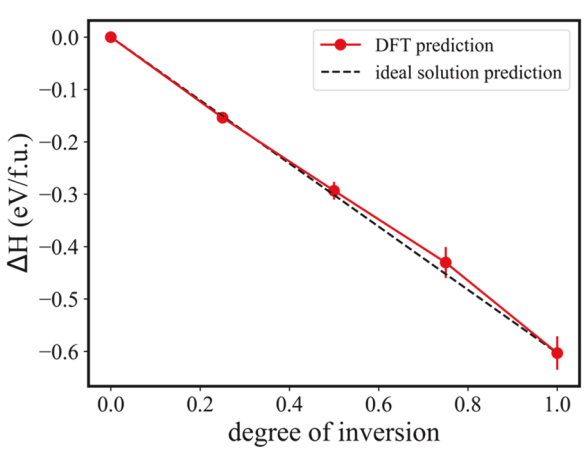

Fig. 1. Variation of formation enthalpy of spinel $NiFe_2O_4$ crystal as a function of degree of inversion.

computational prediction of 0.75 eV/f.u. [38] and 0.74 eV/f.u. [39], and also consistent with the reported experimental observation that $NiFe_2O_4$ shows an approximately inverse structure at equilibrium. For example, El-Sayed et al. observed that synthesized $NiFe_2O_4$ has an inverse spinel structure using both Mössbauer spectra analysis and the Bertaut method [17].

In Table 3, the calculated magnetic moments of the cations in spinel $NiFe_2O_4$ with various degrees of inversion are reported. For the inverse $NiFe_2O_4$, the predicted values of 1.728 μ_B for the Ni ions at the octahedral sites, 4.099 μ_B for the Fe ions at the tetrahedral sites, and 4.195 μ_B for the Fe ions at the octahedral sites are very close to the previous DFT calculation results (1.8 μ_B for the Ni ions at the octahedral sites, 4.11 μ_B for the Fe ions at the tetrahedral sites and 4.2 μ_B for the Fe ions at the octahedral sites [34]). Moreover, the results in Table 3 show that the total magnetic moment per formula of spinel $NiFe_2O_4$ decreases with the degree of inversion, varying from 8.0 μ_B in the normal structure to 2.0 μ_B in the inverse structure. Consequently, DFT reesults demonstrate that both the formation enthalpy and magnetic moment of spinel $NiFe_2O_4$ decrease linearly with an increase in the degree of inversion of the crystal.

3.2. Analysis of chemical bonds in spinel $NiFe_2O_4$

To understand the relation between the system energy and degree of inversion, the types and numbers of different cation-oxygen-cation (i.e., M_1-O-M_2) bonds in spinel $NiFe_2O_4$ were further examined. It is conventionally believed that the magnetic moment interaction between two metal ions is determined by the length and angle of the M_1-O-M_2 bond formed by two metal ions linked through an oxygen ion [40]. For clarity, the different types of M_1-O-M_2 bonds in spinel crystal are distinguished in form of M_1-O-M_2-angle in which M_1 is closer to O than M_2. To find all M_1-O-M_2 bonds in a spinel crystal, all cations near an oxygen ion to form single M-O bonds are first listed. It was found, in an unrelaxed normal spinel $NiFe_2O_4$, that the single M-O bonds had four possible lengths, namely, around 1.84 Å, 2.12 Å, 3.54 Å, and 3.68 Å. Furthermore, two single M-O bonds linking to the same oxygen ion are combined into a M_1-O-M_2 bond whose bond angle is determined by the directional vectors from O to M_1 and from O to M_2. In an unrelaxed normal spinel $NiFe_2O_4$, six distinct types of M_1-O-M_2 bonds, namely, Ni-O-Fe-125$^{o(a)}$, Fe-O-Ni-154°, Ni-O-Fe-180°, Ni-O-Ni-79°, Fe-O-Fe-90°, and Fe-O-Fe-125$^{o(b)}$, are identified as shown in Fig. 2. It should be noted that there are two distinct types of M_1-O-M_2 bonds with the same bond angle of 125°. They are distinguished by using superscripts (a) and (b). In an M_1-O-M_2-125 $^{o(a)}$ bond, the bond lengths are 1.84 Å for M_1-O and 2.12 Å for M_2-O. In an M_1-O-M_2-125 $^{o(b)}$ bond, the bond lengths are 2.12 Å for M_1-O and 3.68 Å for M_2-O.

With an increase in degree of inversion from the normal structure, some Fe ions will occupy the tetrahedral sites and some Ni ions are relocated at the octahedral sites of spinel $NiFe_2O_4$. This structural change induces new types of M_1-O-M_2 bonds in the spinel crystal. For example, all Ni ions will occupy the octahedral sites whereas the Fe ions could be at either the tetrahedral or octahedral sites in an inverse spinel

Table 3
Number and calculated magnetic moment of each type of cations at the tetrahedral (T) and octahedral (O) sites, as well as predicted total magnetic moment in a spinel superlattice containing eight $NiFe_2O_4$ formula and having different degree of inversion. The sign (positive or negative) of the magnetic moment of cations correspond to spin ordering (↑ or ↓) given in Table 1.

Degree of inversion (x)	Number of ions on				Magnetic Moment (μ_B /ion) on				Total Magnetic Moment (μ_B /f.u.)
	T site Ni	O site Ni	T site Fe	O site Fe	T site Ni	O site Ni	T site Fe	O site Fe	
0.00	8	0	0	16	-1.757	–	–	4.264	8.0
0.25	6	2	2	14	-1.752	1.769	-4.087	4.246	6.5
0.50	4	4	4	12	-1.762	1.763	-4.080	4.227	5.0
0.75	2	6	6	10	-1.768	1.743	-4.088	4.210	3.5
1.00	0	8	8	8	–	1.728	-4.099	4.192	2.0

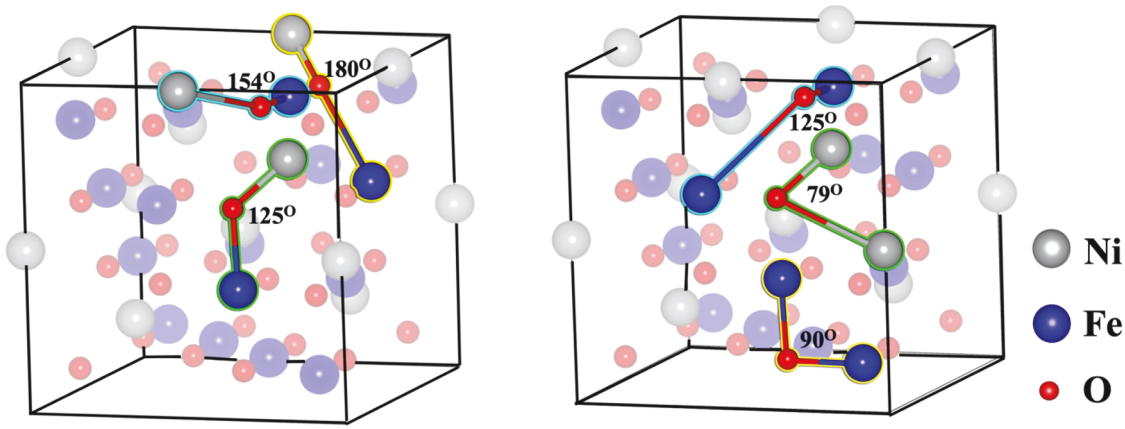

Fig. 2. Schematics showing six distinct types of M_1-O-M_2 bonds in the atomistic structure of a normal spinel $NiFe_2O_4$.

$NiFe_2O_4$. As a result, all the Ni-O-Ni-79° bonds in a normal structure would turn into new Fe-O-Fe-79° bonds in an inverse structure with only Fe ions at the tetrahedral sites. In another example, only one type of Fe-O-Fe-90° bond exists in the normal structure whereas three variations of Fe-O-Fe-90°, Ni-O-Fe-90°, Ni-O-Ni-90° emerge in the inverse structure. The analysis reveals that there are fourteen distinct types of M_1-O-M_2 bonds in an inverse spinel $NiFe_2O_4$. Among these bonds, twelve new types of bonds, namely, Fe-O-Fe-79°, Ni-O-Fe-90°, Ni-O-Ni-90°, Fe-O-Ni-125 $^{o(a)}$, Fe-O-Fe-125$^{o(a)}$, Fe-O-Ni-125$^{o(b)}$, Ni-O-Fe-125$^{o(b)}$, Ni-O-Ni-125° $^{(b)}$, Fe-O-Fe-154°, Ni-O-Fe-154°, Fe-O-Fe-180°, and Fe-O-Ni-180°, appear in the inverse structure but do not exist in the normal structure of $NiFe_2O_4$.

Table 4 summarizes the calculated average numbers of various M_1-O-M_2 bonds in spinel $NiFe_2O_4$ with different degree of inversion (x). It should be noted that the numbers of bonds in Table 4 are the values averaged over 5000 randomly generated configurations of a superlattice containing eight-formula $NiFe_2O_4$. In the structure with $0.0 < x < 1.0$, there exist five new types of bonds (i.e., Fe-O-Ni-79°, Ni-O-Fe-79°, Ni-O-Ni-125$^{o(a)}$, Ni-O-Ni-154°, and Ni-O-Ni-180°) which do not appear in either the normal or inverse structures. The emergence of Fe-O-Ni-79° and Ni-O-Fe-79° bonds occurs because both Fe and Ni ions occupy the tetrahedral sites. The occurrence of Ni-O-Ni-125$^{o(a)}$, Ni-O-Ni-154°, and Ni-O-Ni-180° bonds is because the Ni ions occupy both the tetrahedral and octahedral sites. The number of bonds also varies with degree of inversion. For example, the number of Fe-O-Fe-79° bonds strictly increases whereas that of Fe-O-Fe-125$^{o(b)}$ bonds strictly decreases with increasing degree of inversion. Consequently, the bond analysis reveals the type and number of the M_1-O-M_2 bonds in spinel $NiFe_2O_4$ will vary as a function of degree of inversion which underlies the predicted variation of materials properties reported in Section 3.1.

3.3. Relation between system energy and chemical bonds

In this study, machine learning techniques were applied to derive the relation between the system energy and M_1-O-M_2 chemical bonds of spinel $NiFe_2O_4$. As depicted in Fig. 3, a dataset containing the information of the numbers of different types of the M_1-O-M_2 bonds and the DFT calculated system energies of forty-nine spinel $NiFe_2O_4$ crystal were first constructed. Specifically, there is one spinel structure with $x = 0.00$, one structure with $x = 0.25$, fifteen distinct structures with $x = 0.50$, fifteen distinct structures with $x = 0.75$, and seventeen distinct structures with $x = 1.00$ in the dataset. In this study, the type and number of the M_1-O-M_2 bonds in spinel $NiFe_2O_4$ are selected as the structural features and the system energy of the crystal as the target variable for machine learning (Fig. 3). Thus, a 23-dimensional vector was used to represent a spinel $NiFe_2O_4$ crystal and the magnitude of each dimension to represent the number of a specific type of M_1-O-M_2 bonds in the crystal.

Assuming a linear relation between the bond numbers and crystal energy, the linear regression approach was employed to determine the corresponding energy of each type of the M_1-O-M_2 bonds. The training and test RMSE of the linear regression were found to be 0.00035 eV/atom and 0.00256 eV/atom, respectively. The data points in Fig. 4**a** show only slight scattering around the reference line, indicating the good performance of the linear regression approach for the prediction of spinel $NiFe_2O_4$ energy. In a further test, the DFT-calculated and ML-predicted energies of another ten randomly picked $NiFe_2O_4$ crystal structures were compared. The averaged difference between the DFT and ML predicted energies was found to be just 0.00066 eV/atom and the maximum energy difference among the ten structures was 0.00118 eV/atom. The small difference between the DFT-calculated and ML-predicted energies demonstrates the reliability of the derived structure-energy relation and the representativeness of the structure database employed.

To examine the reliability of the linear relation approximation, a neural network approach was further applied to the same database. The neural network approach assumes a nonlinear relation between the bond numbers and crystal energy and consists of the input layer, hidden

Table 4
Summary of the types, numbers, and bond lengths of M_1-O-M_2 bonds in spinel $NiFe_2O_4$ at different degree of inversion (x) ranging from 0.00 to 1.00. The lengths of M_1-O and M_2-O bonds are given in terms of the lattice parameter a of spinel $NiFe_2O_4$.

	0.00	0.25	0.50	0.75	1.00	M_1-O	M_2-O
Fe-O-Fe-79°	–	3	21	51	96	$\frac{\sqrt{3}}{8}a$	$\frac{\sqrt{11}}{8}a$
Fe-O-Ni-79°	–	21	27	21	–	$\frac{\sqrt{3}}{8}a$	$\frac{\sqrt{11}}{8}a$
Ni-O-Fe-79°	–	21	27	21	–	$\frac{\sqrt{3}}{8}a$	$\frac{\sqrt{11}}{8}a$
Ni-O-Ni-79°	96	51	21	3	–	$\frac{\sqrt{3}}{8}a$	$\frac{\sqrt{11}}{8}a$
Ni-O-Fe-90°	–	22	38	48	52	$\frac{1}{4}a$	$\frac{1}{4}a$
Fe-O-Fe-90°	96	73	53	36	22	$\frac{1}{4}a$	$\frac{1}{4}a$
Ni-O-Ni-90°	–	1	4	12	22	$\frac{1}{4}a$	$\frac{1}{4}a$
Ni-O-Fe-125°[(a)]	96	63	36	15	–	$\frac{\sqrt{3}}{8}a$	$\frac{1}{4}a$
Fe-O-Ni-125°[(a)]	–	3	12	27	48	$\frac{\sqrt{3}}{8}a$	$\frac{1}{4}a$
Fe-O-Fe-125°[(a)]	–	21	36	45	48	$\frac{\sqrt{3}}{8}a$	$\frac{1}{4}a$
Ni-O-Ni-125°[(a)]	–	9	12	9	–	$\frac{\sqrt{3}}{8}a$	$\frac{1}{4}a$
Fe-O-Ni-125°[(b)]	–	22	38	48	51	$\frac{1}{4}a$	$\frac{\sqrt{3}}{4}a$
Ni-O-Fe-125°[(b)]	–	22	38	48	51	$\frac{1}{4}a$	$\frac{\sqrt{3}}{4}a$
Fe-O-Fe-125°[(b)]	192	146	106	72	45	$\frac{1}{4}a$	$\frac{\sqrt{3}}{4}a$
Ni-O-Ni-125°[(b)]	–	2	10	24	45	$\frac{1}{4}a$	$\frac{\sqrt{3}}{4}a$
Fe-O-Ni-154°	96	63	36	15	–	$\frac{1}{4}a$	$\frac{\sqrt{11}}{8}a$
Fe-O-Fe-154°	–	21	36	45	48	$\frac{1}{4}a$	$\frac{\sqrt{11}}{8}a$
Ni-O-Fe-154°	–	3	12	27	48	$\frac{1}{4}a$	$\frac{\sqrt{11}}{8}a$
Ni-O-Ni-154°	–	9	12	9	–	$\frac{1}{4}a$	$\frac{\sqrt{11}}{8}a$
Ni-O-Fe-180°	32	21	12	5	–	$\frac{\sqrt{3}}{8}a$	$\frac{\sqrt{3}}{4}a$
Fe-O-Fe-180°	–	7	12	15	16	$\frac{\sqrt{3}}{8}a$	$\frac{\sqrt{3}}{4}a$
Fe-O-Ni-180°	–	1	4	9	16	$\frac{\sqrt{3}}{8}a$	$\frac{\sqrt{3}}{4}a$
Ni-O-Ni-180°	–	3	4	3	–	$\frac{\sqrt{3}}{8}a$	$\frac{\sqrt{3}}{4}a$

layers, and output layer with a series of neurons in each layer. During the training process, each neuron in the hidden layers transforms the values from the previous layer by a weighted linear summation followed by a non-linear activation function. As shown in Fig. 4**b**, the training and test error of the neural network approach were found to be 0.00045 eV/atom and 0.00234 eV/atom, respectively. Hence, the difference in the errors of the linear regression and neural network models is very small and merely 0.00022 eV/atom, indicating that the linear relation approximation for the bond numbers and system energy is quite reliable for spinel $NiFe_2O_4$.

3.4. *Equilibrium cation distribution in spinel $NiFe_2O_4$*

Taking advantage of the machine-learning derived linear relation between system energy and chemical bonds, a Monte Carlo simulation method has been further applied to predict the cation distribution of spinel $NiFe_2O_4$ equilibrated as a function of temperature. Here, the linear regression ML model was used to predict the energy change associated with structural evolution during the MC simulation, and the MC simulation was used to sample the possible structural configurations in an equilibrium ensemble at a given temperature. The MC simulations were performed in a model cell containing eight formula of $NiFe_2O_4$ (i.e., 56 ions in total).

Using the MC simulations, the equilibrium degree of inversion of $NiFe_2O_4$ could be predicted at elevated temperatures. The normal structure ($x = 0.0$) of $NiFe_2O_4$ was chosen as the initial structure in the MC simulations. The equilibrium degree of inversion was evaluated as the value averaged over 500 equilibrium structures sampled every 100 MC iterations during the last 50,000 iterations of the MC simulations at 1523 K and 1640 K. As shown in Fig. 5**a**, the degree of inversion of $NiFe_2O_4$ would increase whereas the energy of the crystal would decrease in the initial stage of the MC simulations. After 50,000 MC steps, the modeled system reached the thermodynamically equilibrium states with both degree of inversion and energy of $NiFe_2O_4$ fluctuating around equilibrium values, as shown in Fig. 5**b**. From the MC simulations at 1523 K, the equilibrium value for the degree of inversion of $NiFe_2O_4$ was calculated to be 0.996. In comparison, El-Sayed et al. reported an experimental value of 1.0 in Ref [17] for $NiFe_2O_4$ annealed at 1523 K. From the MC simulations at 1640 K, the equilibrium value for the degree of inversion of $NiFe_2O_4$ was calculated to be 0.991, agreeing well with the experimental value of 0.992 [39]. In comparison, the thermodynamic model by Navrotsky et al. gave an underestimated value of 0.988 for the equilibrium degree of inversion at 1640 K [39]. It should be pointed out that the presented computational approach neglects the

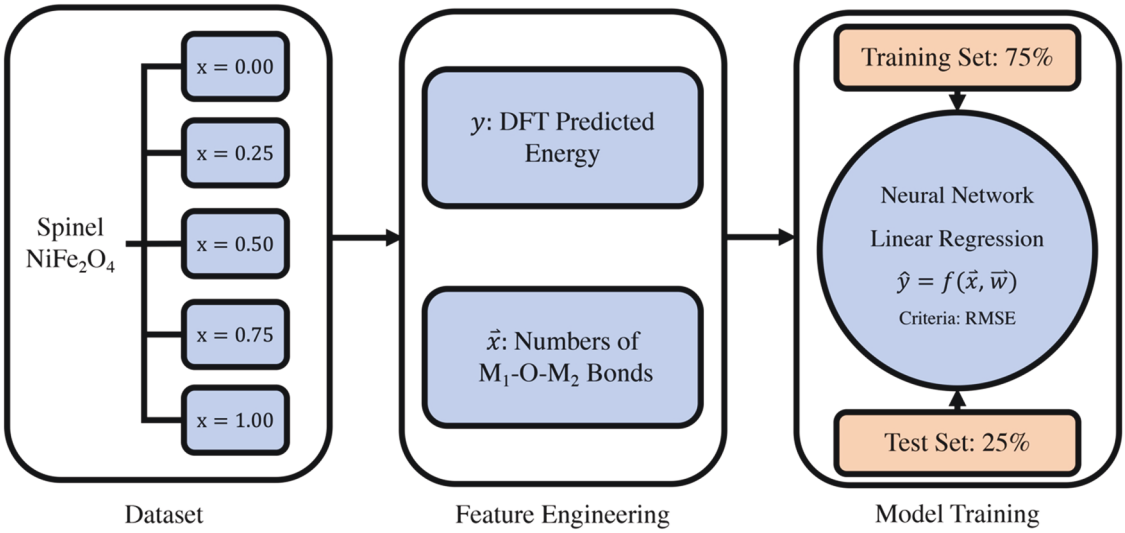

Fig. 3. Schematics of machine learning approach.

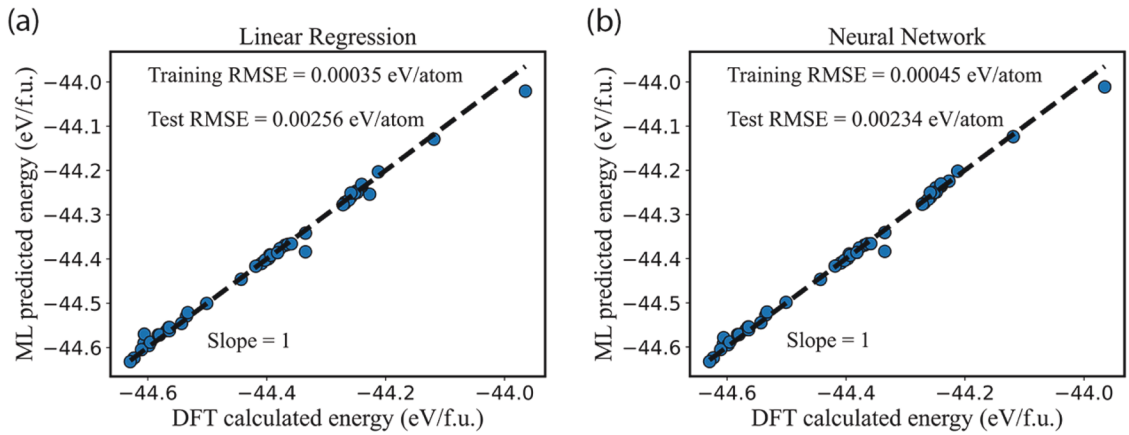

Fig. 4. DFT calculated energies as compared to predicted energies from (a) linear regression and (b) neural network machine learning models.

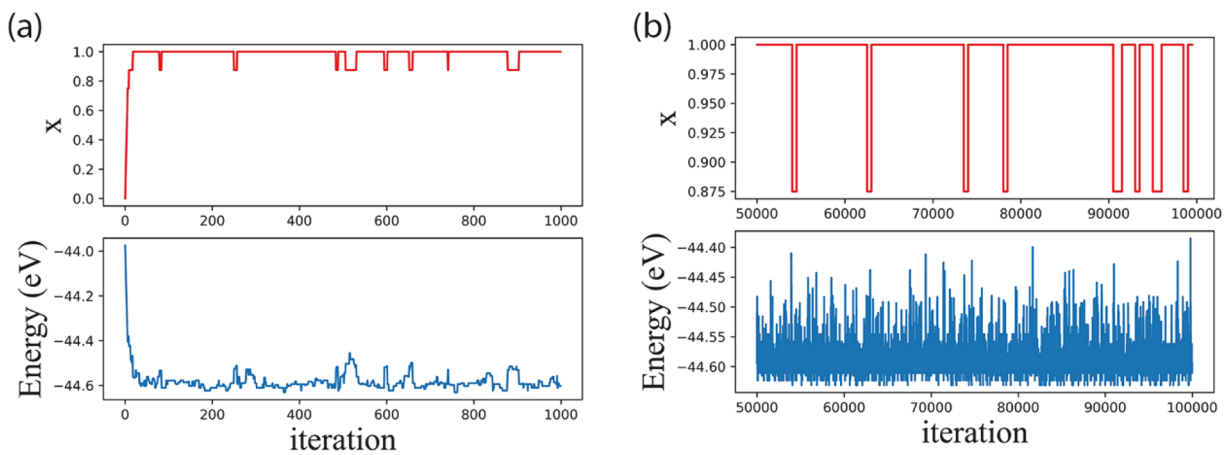

Fig. 5. Evolution of degree of inversion and system energy in (a) the first 1000 iterations and (b) the last 50,000 iterations of the MC simulation at 1640 K.

influence of vibrational entropy on the cation distribution. This assumption can yield some discrepancy between prediction and measurement, especially at high temperatures. However prior experimental studies [39] have concluded that configurational entropy is dominant as it relates to cation site occupation when determining interchange enthalpy of spinel oxides and so the assumptions are consistent with experimental results reported.

For the inverse spinel crystal, there is another transition which turns an ordered cation distribution into a disordered one through the position exchange of different cations at the octahedral sites only [41,42]. Raman spectra measurement [43] revealed that the single crystal of inverse spinel $NiFe_2O_4$ exhibited a symmetry with tetragonal $P4_122$ space group in which the Fe and Ni ions should alternatively occupy the octahedral sites along the [1 1 0] and [1 $\bar{1}$ 0] directions in an ordered fashion. In addition, the first-principles calculations predicted that such an ordered structure had the lowest system energy and was thus the preferred structure of the inverse spinel $NiFe_2O_4$ at low temperature [38,44]. By contrast, the inverse spinel $NiFe_2O_4$ could exhibit a cubic $Fd\bar{3}m$ symmetry, in which the Fe and Ni ions randomly occupy the octahedral sites at high temperature. Distinguishing these two types of inverse spinel $NiFe_2O_4$, an ordering parameter is defined to be the occupancies of Fe ions at the octahedral Fe sites as in the $P4_122$ ordered inverse $NiFe_2O_4$. Hence, the value of the ordering parameter changes from 1.0 for an ordered cation distribution in the $P4_122$ inverse structure to 0.50 for a disordered cation distribution in the $Fd\bar{3}m$ inverse structure. In this study, the Monte Carlo simulation method was further applied to predict this order-disorder transition in the inverse structure of spinel $NiFe_2O_4$.

The initial structure in the MC simulations was chosen to be the inverse spinel $NiFe_2O_4$ with the ordered $P4_122$ symmetry. During the MC simulations with 100,000 iterations, the positions of a pair of randomly selected Ni and Fe ions at the octahedral sites were attempted to exchange. The MC simulations were performed at the temperature range from 100 K to 230 K. The values of the ordering parameter were evaluated every 100 MC steps during the last 10,000 steps of the MC simulation at each temperature. As shown in Fig. 6, the average value of

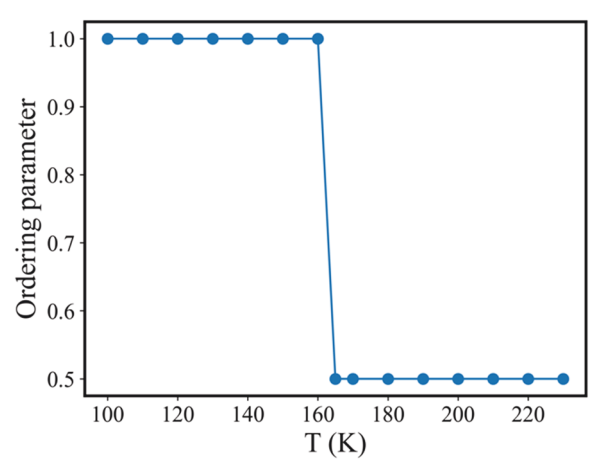

Fig. 6. Predicted variation of ordering parameter as a function of temperature in inverse spinel $NiFe_2O_4$ from MC simulations.

the ordering parameter changes from 1.0 to 0.5 at around 165 K. Thus, the transition temperature from an ordered to disordered cation distribution in the inverse structure of spinel $NiFe_2O_4$ is predicted to be about 165 K. It should be mentioned that Dey et al. used synchrotron diffraction technique and determined this order-disorder transition temperature of the inverse spinel $NiFe_2O_4$ to be around 98 K [45]. In the MC simulations, the perfect $NiFe_2O_4$ single crystal without any structural defects such as the vacancies at the octahedral sites were considered. This may explain the discrepancy between the computational and experimental values.

4. Conclusion

In this study, relevant physical properties (i.e., system energy, lattice parameter, and atomic magnetic moment) of spinel $NiFe_2O_4$ crystal varying as a function of its cation distribution (i.e., degree of inversion x) were predicted using the first-principles DFT calculations. The DFT results show that $NiFe_2O_4$ crystal would have the lowest system energy in an inverse spinel structure ($x = 1.0$) whereas the highest energy in a normal structure ($x = 0.0$). Moreover, the total magnetic moment per formula of spinel $NiFe_2O_4$ decreases with the degree of inversion, varying from 8.0 μ_B in the normal structure to 2.0 μ_B in the inverse structure. Consequently, the calculation results indicate a clear correlation between the physical properties and degree of inversion in spinel $NiFe_2O_4$, which is consistent with prior experimental investigations. Furthermore, the bond analysis on spinel $NiFe_2O_4$ crystal was performed. It is found the number of distinct types of M_1-O-M_2 bonds is six in a normal structure, fourteen in an inverse structure, and twenty-three in the structures with $0 < x < 1$. Moreover, the number of each type of M_1-O-M_2 bonds is found to vary with degree of inversion. As indicated in Table 4, the number of Fe-O-Fe-79° bonds strictly increases whereas that of Fe-O-Fe-125$^{o(b)}$ bonds strictly decreases with increasing degree of inversion.

Moreover, the relation between the system energy and chemical bonds of spinel $NiFe_2O_4$ was deduced using both linear regression and neural network machine learning methods. It is found that there is a linear relation between the system energy and the number of each type of M_1-O-M_2 bonds. Taking advantage of this linear relation, an ML method could be used to accurately predict the energy of different structures of spinel $NiFe_2O_4$ crystal. The efficient ML method for energy prediction enables sampling a large amount of equilibrium structures of spinel $NiFe_2O_4$ using the Monte Carlo simulations. Specifically, this DFT data informed, machine learning enabled Monte Carlo simulation method was applied to predict the value of degree of inversion of spinel $NiFe_2O_4$ in thermodynamically equilibrium states at 1523 K and 1640 K, and the transition temperature for an ordered to disordered cation distribution in the inverse structure of spinel $NiFe_2O_4$. The computational predictions are found to agree well with experimental results, validating the reliability of the proposed computational approach.

Therefore, the developed bond analysis method and efficient machine learning enabled Monte Carlo simulation would be critical computational tools for future studies which seek to predict how equilibrium cation distribution in other complex spinel crystal would vary appreciably as a function of annealing temperature.

CRediT authorship contribution statement

Ying Fang: Investigation, Method development, Data curation, Writing – original draft. **Siming Zhang:** Data curation, Writing – review & editing. **Paul R. Ohodnicki:** Conceptualization, Supervision, Writing – review & editing. **Guofeng Wang:** Conceptualization, Supervision, Writing – review & editing.

Declaration of Competing Interest

The authors declare that they have no known competing financial interests or personal relationships that could have appeared to influence the work reported in this paper.

Data availability

Data will be made available on request.

Acknowledgments

Wang acknowledges the support from U.S. National Science Foundation (NSF DMR #1905572). Ohodnicki gratefully acknowledges support from the Office of Naval Research (ONR GRANT #13330021). The authors also gratefully acknowledge the computational resources provided by the Center for Research Computing of the University of Pittsburgh and the Extreme Science and Engineering Discovery Environment (XSEDE).

References

[1] S.B. Narang, K. Pubby, Nickel spinel ferrites: a review, J. Magn. Magn. Mater. 519 (2021), 167163.
[2] A. Talaat, M. Suraj, K. Byerly, A. Wang, Y. Wang, J. Lee, P. Ohodnicki Jr, Review on soft magnetic metal and inorganic oxide nanocomposites for power applications, J. Alloy. Compd. 870 (2021), 159500.
[3] F.C. Oliveira, F.B. Effenberger, M.H. Sousa, R.F. Jardim, P.K. Kiyohara, J. Dupont, J.C. Rubim, L.M. Rossi, Ionic liquids as recycling solvents for the synthesis of magnetic nanoparticles, Phys. Chem. Chem. Phys. 13 (2011) 13558–13564.
[4] P.V. Kumar, M.P. Short, S. Yip, B. Yildiz, J.C. Grossman, High surface reactivity and water adsorption on $NiFe_2O_4$ (111) surfaces, J. Phys. Chem. C 117 (2013) 5678–5683.
[5] J. Patil, D. Nadargi, J. Gurav, I. Mulla, S. Suryavanshi, Synthesis of glycine combusted $NiFe_2O_4$ spinel ferrite: a highly versatile gas sensor, Mater. Lett. 124 (2014) 144–147.
[6] S. Permien, T. Neumann, S. Indris, G. Neubüser, L. Kienle, A. Fiedler, A.-L. Hansen, D. Gianolio, T. Bredow, W. Bensch, Transition metal cations on the move: simultaneous operando X-ray absorption spectroscopy and X-ray diffraction investigations during Li uptake and release of a $NiFe_2O_4$/CNT composite, Phys. Chem. Chem. Phys. 20 (2018) 19129–19141.
[7] S.B. Bandgar, M.M. Vadiyar, Y.-C. Ling, J.-Y. Chang, S.-H. Han, A.V. Ghule, S. S. Kolekar, Metal precursor dependent synthesis of $NiFe_2O_4$ thin films for high-performance flexible symmetric supercapacitor, ACS Appl. Energy Mater. 1 (2018) 638–648.
[8] K. Shetty, L. Renuka, H.P. Nagaswarupa, H. Nagabhushana, K.S. Anantharaju, D. Rangappa, S.C. Prashantha, K. Ashwini, A comparative study on $CuFe_2O_4$, $ZnFe_2O_4$ and $NiFe_2O_4$: morphology, impedance and photocatalytic studies, Mater. Today Proc. 4 (2017) 11806–11815.
[9] H.S. Kim, D. Kim, B.S. Kwak, G.B. Han, M.-H. Um, M. Kang, Synthesis of magnetically separable core@shell structured $NiFe_2O_4$@TiO_2 nanomaterial and its use for photocatalytic hydrogen production by methanol/water splitting, Chem. Eng. J. 243 (2014) 272–279.
[10] C. Xiangfeng, J. Dongli, Z. Chenmou, The preparation and gas-sensing properties of $NiFe_2O_4$ nanocubes and nanorods, Sens. Actuators B Chem. 123 (2007) 793–797.
[11] C.-S. Hsu, N.-T. Suen, Y.-Y. Hsu, H.-Y. Lin, C.-W. Tung, Y.-F. Liao, T.-S. Chan, H.-S. Sheu, S.-Y. Chen, H.M. Chen, Valence-and element-dependent water oxidation behaviors: in situ X-ray diffraction, absorption and electrochemical impedance spectroscopies, Phys. Chem. Chem. Phys. 19 (2017) 8681–8693.
[12] C.T. Cherian, J. Sundaramurthy, M. Reddy, P. Suresh Kumar, K. Mani, D. Pliszka, C. H. Sow, S. Ramakrishna, B. Chowdari, Morphologically robust $NiFe_2O_4$ nanofibers as high capacity Li-ion battery anode material, ACS Appl. Mater. Interfaces 5 (2013) 9957–9963.
[13] M. Harada, M. Kuwa, R. Sato, T. Teranishi, M. Takahashi, S. Maenosono, Cation distribution in monodispersed MFe_2O_4 (M= Mn, Fe, Co, Ni, and Zn) nanoparticles investigated by X-ray absorption fine structure spectroscopy: implications for magnetic data storage, catalysts, sensors, and ferrofluids, ACS Appl. Nano Mater. 3 (2020) 8389–8402.
[14] V. Šepelák, I. Bergmann, A. Feldhoff, P. Heitjans, F. Krumeich, D. Menzel, F. J. Litterst, S.J. Campbell, K.D. Becker, Nanocrystalline nickel ferrite, $NiFe_2O_4$: mechanosynthesis, nonequilibrium cation distribution, canted spin arrangement, and magnetic behavior, J. Phys. Chem. C 111 (2007) 5026–5033.
[15] K.R. Sanchez-Lievanos, J.L. Stair, K.E. Knowles, Cation distribution in spinel ferrite nanocrystals: characterization, impact on their physical properties, and opportunities for synthetic control, Inorg. Chem. 60 (2021) 4291–4305.
[16] Ž. Cvejić, E. Đurđić, G.I. Ivandekić, B. Bajac, P. Postolache, L. Mitoseriu, V. Srdić, S. Rakić, The effect of annealing on microstructure and cation distribution of $NiFe_2O_4$, J. Alloy. Compd. 649 (2015) 1231–1238.
[17] K. El-Sayed, M.B. Mohamed, S. Hamdy, S. Ata-Allah, Effect of synthesis methods with different annealing temperatures on micro structure, cations distribution and magnetic properties of nano-nickel ferrite, J. Magn. Magn. Mater. 423 (2017) 291–300.

[18] A.B. Nawale, N.S. Kanhe, K. Patil, S. Bhoraskar, V. Mathe, A. Das, Magnetic properties of thermal plasma synthesized nanocrystalline nickel ferrite ($NiFe_2O_4$), J. Alloy. Compd. 509 (2011) 4404–4413.
[19] A. Sinha, M. Singh, S. Achary, A. Sagdeo, D. Shukla, D. Phase, Crystal field splitting and spin states of Co ions in cobalt ferrite with composition $Co_{1.5}Fe_{1.5}O_4$ using magnetization and X-ray absorption spectroscopy measurements, J. Magn. Magn. Mater. 435 (2017) 87–95.
[20] V. Stevanovic, M. d'Avezac, A. Zunger, Universal electrostatic origin of cation ordering in A_2BO_4 spinel oxides, J. Am. Chem. Soc. 133 (2011) 11649–11654.
[21] X. Zhang, A. Zunger, Diagrammatic separation of different crystal structures of A_2BX_4 compounds without energy minimization: a pseudopotential orbital radii approach, Adv. Funct. Mater. 20 (2010) 1944–1952.
[22] G. Tang, D. Ji, Y. Yao, S. Liu, Z. Li, W. Qi, Q. Han, X. Hou, D. Hou, Quantum-mechanical method for estimating ion distributions in spinel ferrites, Appl. Phys. Lett. 98 (2011), 072511.
[23] D. Carta, M.F. Casula, A. Falqui, D. Loche, G. Mountjoy, C. Sangregorio, A. Corrias, A structural and magnetic investigation of the inversion degree in ferrite nanocrystals MFe_2O_4 (M= Mn, Co, Ni), J. Phys. Chem. C 113 (2009) 8606–8615.
[24] D. Ji, G. Tang, Z. Li, X. Hou, Q. Han, W. Qi, S. Liu, R. Bian, Quantum mechanical method for estimating ionicity of spinel ferrites, J. Magn. Magn. Mater. 326 (2013) 197–200.
[25] G. Pilania, V. Kocevski, J.A. Valdez, C.R. Kreller, B.P. Uberuaga, Prediction of structure and cation ordering in an ordered normal-inverse double spinel, Commun. Mater. 1 (2020) 1–11.
[26] G. Kresse, J. Furthmüller, Efficient iterative schemes for ab initio total-energy calculations using a plane-wave basis set, Phys. Rev. B 54 (1996) 11169.
[27] G. Kresse, D. Joubert, From ultrasoft pseudopotentials to the projector augmented-wave method, Phys. Rev. B 59 (1999) 1758.
[28] J.P. Perdew, K. Burke, M. Ernzerhof, Generalized gradient approximation made simple, Phys. Rev. Lett. 77 (1996) 3865.
[29] D.J. Chadi, Special points for Brillouin-zone integrations, Phys. Rev. B 16 (1977) 1746.
[30] A. Van de Walle, P. Tiwary, M. De Jong, D. Olmsted, M. Asta, A. Dick, D. Shin, Y. Wang, L.-Q. Chen, Z.-K. Liu, Efficient stochastic generation of special quasirandom structures, Calphad 42 (2013) 13–18.
[31] F. Pedregosa, G. Varoquaux, A. Gramfort, V. Michel, B. Thirion, O. Grisel, M. Blondel, P. Prettenhofer, R. Weiss, V. Dubourg, Scikit-learn: machine learning in Python, J. Mach. Learn. Res. 12 (2011) 2825–2830.
[32] G. Hackeling. Mastering Machine Learning with scikit-learn, second ed., Packt Publishing Ltd, Birmingham, 2017, pp. 21–50.
[33] H. Perron, T. Mellier, C. Domain, J. Roques, E. Simoni, R. Drot, H. Catalette, Structural investigation and electronic properties of the nickel ferrite $NiFe_2O_4$: a periodic density functional theory approach, J. Phys. Condens. Matter 19 (2007), 346219.
[34] K. Dileep, B. Loukya, N. Pachauri, A. Gupta, R. Datta, Probing optical band gaps at the nanoscale in $NiFe_2O_4$ and $CoFe_2O_4$ epitaxial films by high resolution electron energy loss spectroscopy, J. Appl. Phys. 116 (2014), 103505.
[35] C. O'Brien, Z. Rák, D.W. Brenner, Free energies of (Co, Fe, Ni, Zn) Fe_2O_4 spinels and oxides in water at high temperatures and pressure from density functional theory: results for stoichiometric NiO and $NiFe_2O_4$ surfaces, J. Phys. Condens. Matter 25 (2013), 445008.
[36] U.-G. Jong, C.-J. Yu, Y.-S. Park, C.-S. Ri, First-principles study of ferroelectricity induced by p–d hybridization in ferrimagnetic $NiFe_2O_4$, Phys. Lett. A 380 (2016) 3302–3306.
[37] Y. Hou, Y. Zhao, Z. Liu, H. Yu, X. Zhong, W. Qiu, D. Zeng, L. Wen, Structural, electronic and magnetic properties of partially inverse spinel $CoFe_2O_4$: a first-principles study, J. Phys. D Appl. Phys. 43 (2010), 445003.
[38] D. Fritsch, C. Ederer, Effect of epitaxial strain on the cation distribution in spinel ferrites $CoFe_2O_4$ and $NiFe_2O_4$: A density functional theory study, Appl. Phys. Lett. 99 (2011), 081916.
[39] A. Navrotsky, O. Kleppa, The thermodynamics of cation distributions in simple spinels, J. Inorg. Nucl. Chem. 29 (1967) 2701–2714.
[40] A. Goldman. Modern Ferrite Technology, second ed., Springer, New York, 2006, pp. 51–71.
[41] A. Seko, F. Oba, I. Tanaka, Classification of spinel structures based on first-principles cluster expansion analysis, Phys. Rev. B 81 (2010), 054114.
[42] A. Seko, K. Yuge, F. Oba, A. Kuwabara, I. Tanaka, Prediction of ground-state structures and order-disorder phase transitions in II-III spinel oxides: a combined cluster-expansion method and first-principles study, Phys. Rev. B 73 (2006), 184117.
[43] V. Ivanov, M. Abrashev, M. Iliev, M. Gospodinov, J. Meen, M. Aroyo, Short-range B-site ordering in the inverse spinel ferrite $NiFe_2O_4$, Phys. Rev. B 82 (2010), 024104.
[44] D. Fritsch, C. Ederer, First-principles calculation of magnetoelastic coefficients and magnetostriction in the spinel ferrites $CoFe_2O_4$ and $NiFe_2O_4$, Phys. Rev. B 86 (2012), 014406.
[45] J. Dey, A. Chatterjee, S. Majumdar, A.-C. Dippel, O. Gutowski, M.V. Zimmermann, S. Giri, Ferroelectric order associated with ordered occupancy at the octahedral site of the inverse spinel structure of multiferroic $NiFe_2O_4$, Phys. Rev. B 99 (2019), 144412.